Corrosion Behavior Of Aluminium Alloy Aa2219–T87 Welded Plates in Sea Water

G. Venkatasubramanian[a] A. Sheik Mideen[a*], Abhay K Jha[b]

[a]*Department of Chemistry, Sathyabama University, Jeppiaar Nagar, Chennai-*600119*, India*

[b]*Materials Characterization Division, Vikram Sarabhai Space Centre, Indian Space Research Organisation, Trivandrum–*695022*, India*

venkatguru_1966@yahoo.co.in, smideen@yahoo.co.in*

Abstract

The corrosion behavior of aluminium alloy AA2219−T87 welded plates in seawater was investigated using potentiodynamic polarization and EIS techniques. The potentiodynamic polarization curves reveal that heat affected zone (HAZ) is more prone to corrosion than weld zone (WZ) and base metal (BM). This is further confirmed by EIS which showed a decrease of R_{ct}. The microstructures of AA2219−T87 were made by optical microscopy and SEM. The higher environmental susceptibility of HAZ as compared to BM is caused by the dissolution and segregation of $CuAl_2$ intermetallic particles along the grain boundaries. The corrosion rate of WZ is due to the presence of micro pores and copper rich areas in α-matrix.

Keywords: Aluminium, EIS, SEM, Heat Affected Zone

1. Introduction

The most readily weldable high strength aluminium alloy 2219 (Metals Hand Book, 1990, Aluminium standards and data, 1982) in T87 temper condition finds extensive use for the structural construction of cryogenic fuel tanks to store liquid oxygen (−183°C/90K) and liquid hydrogen (−253°C/20K). Its only disadvantage is its poor corrosion resistance especially in chloride containing environment owing to higher copper content.

Over the years, a number of studies have been carried out in order to assess the effect of copper content and the distribution of second phase intermetallic particles on the corrosion behavior of aluminium alloys (Robinson et. al., 1982; Meletis et. al., 1991; Keddam et. al., 1997; Williams Stewart et. al., 2003; Paglia et. al., 2006; Birbilis et. al., 2005). The copper distribution in the microstructure affects the susceptibility to localized corrosion. Pitting corrosion is usually occurs in the Al matrix near copper containing intermetallic particles owing to galvanic interaction with Al matrix (Lunarska et. al., 1987). Intergranular corrosion (IGC) is generally believed to be associated with Cu containing grain boundary precipitates and the PFZ along grain boundaries (Hatch ASM 1984; Ramgopal et. al., 2002).

Attempts have been made to study the corrosion properties of various zones of friction stir welded (FSW), AA2024, AA7075 (Lumsden et. al., 1999; Paglia et. al., 2002; paglia et. al 2003; Lumsden et. al., 2003), AA2017−T4 (Kuznicka et. al., 2008) and the results have shown that the heat affected zone (HAZ) of these aluminium alloys were more susceptible to corrosion than the base metal. Corrosion behavior of Al-Si/Sic composite in sea water was analysed and reported (Gnecco et. al,. 1999). Frankel and Xia (Frankel et. al., 1999) investigated the pitting corrosion and stress corrosion cracking behavior of FSW AA5454 alloy and compared them with those of base alloy and in gas tungsten arc welded (GTAW) samples. Rao et al (Koteswara Rao et. al., 2005) have shown that the copper segregation to grain boundaries has significant effect on pitting corrosion behavior of AA2219 electron beam welds. Liquation in FSW and gas metal arc welded (GMAW) AA2219 has been investigated by Cao et al (Cao et. al., 2005; Huang C et. al., 2004). GMAW AA2219 showed that θ ($CuAl_2$) particles acts as insitu microsensors for detecting the onset of liquation by forming distinct composite like eutectic particles upon reaching the eutectic temperature. The general corrosion resistance of the weld nugget was better than that of the parent AA2219 friction stir weldment in 3.5% NaCl solution (Balasrinivasan et. al., 2010). Corrosion behavior of aluminium alloy 2219 treated with a chromate conversion coating exposed to 3.5% NaCl was investigated by Rossana Grilli (Rossana Grilli et. al., 2011). The accumulative roll bonding (ARB) of dissimilar aluminum alloys AA2219 and AA5086 was reported recently by Shibayan Roy (Shibayan Roy et. al., 2012). Atmospheric corrosion of aluminium alloy 2024-T3 exposed to salt lakes environment for 6 years was investigated recently (B.B. Wang et. al., 2012).

Most of the corrosion studies investigated so far is pertaining to FSW aluminium alloys. Electrochemical corrosion and SCC behavior of TIG welded AA2219 Aluminium alloy in 3.5 Wt. pct. NaCl solution was reported by Venugopal (Venugopal et. al., 2010). Among the available welding processes, GTAW process on AC mode with 2319 filler wire is largely followed for welding because of its inherent advantages of arc cleaning (Ghosh et. al., 2007). The present work elucidates the corrosion behavior of different zones namely, weld zone (WZ) and heat affected zone (HAZ) of gas tungsten arc welded AA2219−T87 plates in sea water and compared the results with base metal (BM) in T87 temper condition.

2. Experimental

Gas tungsten arc welded (GTAW) AA2219 rolled plate of size 570mm × 500mm × 7.4mm in T−87 temper condition (Fig.1) was used in the present study. The temper designation T8 represents solution heat treatment and cold working followed by artificial aging and 7 represents the percentage of cold work employed (Aluminium standards and data'1982). The gas tungsten arc welding process on alternating current mode with ER 2319 alloy (filler wire) is used for welding the rolled plates and the procedure is described elsewhere (Venkata Narayana et al., 2004). The chemical composition of parent metal and weld filler wire are given in Table 1.

The working electrodes for corrosion studies were cut from the welded plates in transverse direction parallel to the rolling direction and perpendicular to welding direction in such a way the test specimens consisted of base metal (BM), weld zone (WZ) and heat affected zone (HAZ). The specimens were used in flat type after flush grinding both the crown and root beads with mirror smooth finish after polished with different grades of silicon carbide sheets followed by 1 µm finish using rotating disc with non-aqueous diamond paste, degreased by acetone, washed with double distilled water and dried. Except the zone under study, the rest of the zones were suitably masked with a red lacquer and further wrapped with Teflon tape. The Keller etchant [2.5ml HNO_3 (60%) + 1.5ml HCl (37%) + 1ml HF (48%) + 95 ml of double distilled water] was used to identify the HAZ and are located 3 mm away from weld zones on both sides. In all experiments 8mm×1mm was exposed in order to compare the results.

Potentiodynamic polarization tests were carried out according to ASTM standard G3–89 (ASTM G3-89,2004)) using software based Bio-analytical system [BAS−Zahner, make IM6–electrochemical analyzer model using THALAS−Flink software]. The flat type working electrodes were categorized into BM, WZ and HAZ. A saturated calomel electrode coupled to a fine Luggin capillary as reference electrode and graphite electrode as counter electrode were used. The Luggin capillary was kept close to the working electrode to reduce the ohmic contribution. Sea water (pH = 8.23) collected from East Coast area, Chennai was used as electrolyte. The polarization curves were determined by stepping the potential at a scan rate of 0.5 mV/sec. from –250 mV (SCE) to +250 mV vs SCE. All the experiments analyzed in this paper were performed at room temperature (25°C) and repeated for at least two times to get reproducibility.

The electrochemical impedance spectroscopy (EIS) measurements were carried out in sea water using a potentiostat coupled to a frequency response analyzer system in the frequency range 100 k Hz. to 100 m Hz with a sinusoidal perturbation of 10 mV at OCP. The working electrode consists of either BM or WZ or HAZ and graphite electrode and saturated calomel electrode were used as counter electrode and reference electrode respectively. Potentiodynamic polarization and EIS measurements were performed after initial delay of 10 minutes for the sample to reach a steady state condition.

Fig.1. *Locations of test specimens of Base metal (BM), heat affected zones (HAZ),weld zone (WZ)*

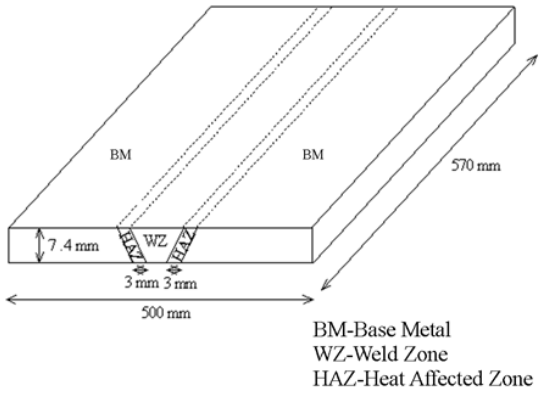

Table 1. *Nominal composition of AA2219-T87 and ER2319 filler metal (% by mass)*

Alloy	Elements %							
	Cu	Mn	Zr	V	Ti	Fe	Si	Al
AA2219	5.95	0.27	0.12	0.09	0.06	0.12	0.05	Balance
ER2319	6.10	0.29	0.15	0.1	0.15	0.10	0.04	Balance

The microstructure of the AA2219−T87 welded plates were characterized by using optical microscopy (Olympus GX 71 Inverted Metallurgical Microscope, Japan) and Scanning Electron Microscopy (SEM). Optical metallography was performed on samples with transverse cross section. The samples were polished with different grade of silicon carbide sheets followed by 1 µm finish using rotating disc with non-aqueous diamond paste followed by etching with Keller's etchant for about 30 to 60 seconds and used. SEM characterization was performed on samples using scanning electron microscope (HITACHI model) operating at 15kV.

3. Results and discussions

3.1 Potentiodynamic polarization tests

Fig.2 shows the potentiodynamic polarization curves for BM, WZ and HAZ of AA2219−T87 welded plate in natural sea water. Table 2 summarizes the various corrosion parameters obtained from Tafel plots.

The open circuit potential for the regions of HAZ, WZ and BM in sea water showed the values –645 mV, –659 mV and –680 mV respectively. These values mainly depend on the chemical composition of the base alloy and filler metal used.

The values of corrosion potential (E_{corr}) for BM when compared to WP and HAZ exhibits a little shift towards anodic side. This shift was confirmed in the reduction of corrosion current density (i_{corr}) 0.156 µA cm^{-2}. The E_{corr} towards anodic side and reduction in i_{corr} may be due to higher anodic to cathodic area distribution (Holingsworth, ASM handbook 2001). It is clear from polarization

curves that, all regions showed cathodic control reaction since they have higher cathodic Tafel slopes than anodic Tafel slopes. The predominance of cathodic Tafel slope is due to the presence of main alloying element copper and second phase intermetallic particles $CuAl_2$. A little passive region can be observed from the anodic side of all regions is due to the slightly higher pH of sea water.

Fig.2. *Anodic and cathodic polarization curves for AA 2219-T87 in seawater*

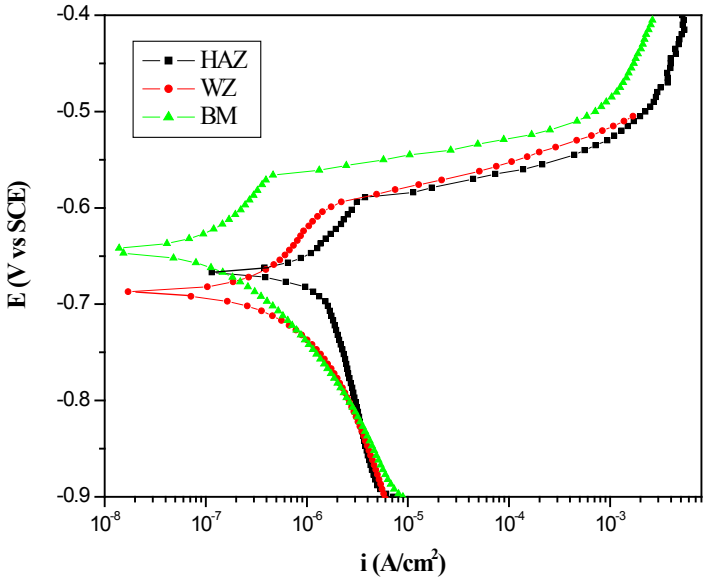

Table 2. *Corrosion parameters obtained from Tafel plots for different zones of AA2219-T87 welded plates in sea water*

Various Zones	OCP (V vs SCE)	i_{corr} (μA cm-2)	β_a (mV dec-1)	β_c (mV dec-1)	E_{corr} (V vs SCE)
BM	-0.680	0.156	111	-151	-0.644
WZ	-0.659	0.555	120	-225	-0.688
HAZ	-0.645	1.22	114	-411	-0.653

The E_{corr} for WZ and HAZ exhibits a shift towards cathodic side from OCP (−659 mV to –688 mV for WZ and –645 mV to –653 mV for HAZ). This shift indicates that corrosion of these regions follow via cathodic dissolution mechanism. This factor is further supported by i_{corr} which is 0.555 μA cm^{-2} for WZ and 1.22 μA cm^{-2} for HAZ. During welding the temperature in the HAZ varies from 490°C to 570°C. Due to this high temperature the dissociation and segregation of hardening precipitates, $CuAl_2$ takes place along the grain boundaries (Koteswara Rao et. al., 2005). Further this causes redistribution and enrichment of copper in HAZ when exposed to sea water. These enriched copper acts as pure cathode and supports oxygen reduction at higher rates (Kuznicka et al., 2008), which greatly lowers alloys corrosion resistance particularly in the HAZ.

4. EIS measurements

Fig.3a illustrates the Nyquist plot obtained for different zones of AA2219−T87 welded plate in sea water. The various corrosion parameters obtained from Nyquist plots are given in Table 3.

The diameter of low frequency capacity loop corresponding to charge transfer resistance indicates the corrosion rate. The BM showed maximum R_{ct} (63 kΩ cm^2) than WZ (23 kΩ cm^2) and HAZ (9 kΩ cm^2). This higher corrosion resistance of parent metal is due to the more homogeneous distribution of $CuAl_2$ intermetallic particles in α-solid solution. This is in agreement with the results provided by Rao et al (Koteswara Rao et. al., 2005). The capacitance connected in parallel to the charge transfer resistance corresponds to interfacial capacitance ((C_{dl}) and therefore may approximately indicate the expanded surface area of the corroding electrode. This was calculated using the following formula

where, is the maximum frequency, obtained from the Nyquist plots. The decrease of the capacitance for BM ($3.41x10^{-3}$μF cm^2) further confirms the increased corrosion resistance in sea water. The relatively lower R_{ct} and increased capacitance showed the lower corrosion resistance of HAZ. This is essentially due to the acceleration of cathodic reaction. Presence of shrinkage pores and copper rich phase in WZ is responsible for low R_{ct}.

Fig.3 (a). *Nyquist plot for AA2219-T87 welded plate in seawater*

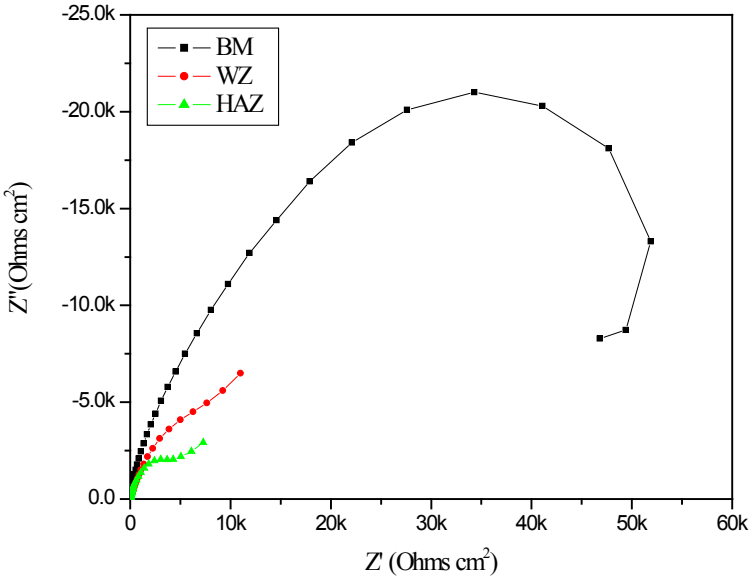

Fig.3b shows experimental EIS results in Bode magnitude diagram for different zones of AA2219−T87 welded plate in sea water. A higher impedance of 48.3 k Ohms cm^2 was obtained for BM compare to WZ (15.7 k Ohms cm^2) and HAZ (8.5 k Ohms cm^2). This is also well agreement with the previous results from Tafel and Nyquist plot. It is known that higher impedance values are conducive to nobler electrochemical behavior. In BM, it is due to more homogenous distribution of fine $CuAl_2$ precipitates in α-solid solution.

Fig.3 (b). *Bode Magnitude plot for AA2219-T87 welded plate in seawater*

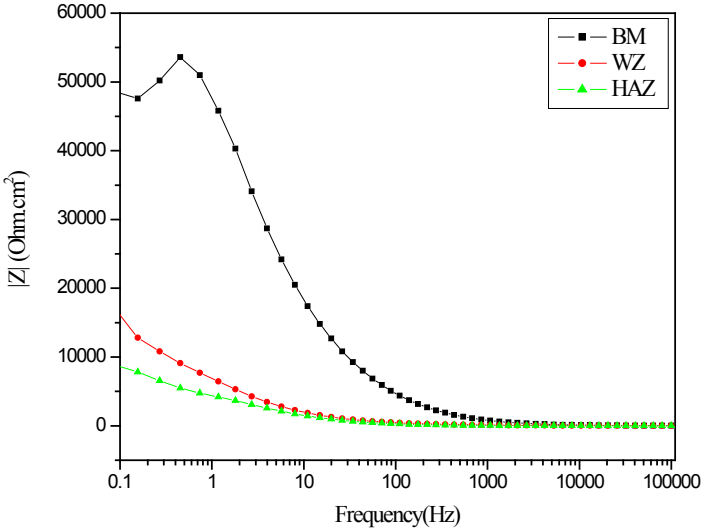

Table 3. *Impedance parameters for different zones of AA2219-T87 welded plates in sea water*

Various Zones	Rct(kΩ cm2)	Cdl(μF cm2)	Imp(k Ohms cm2)
BM	63	3.41x10-3	48.3
WZ	23	5.8x10-3	15.7
HAZ	9	1.4x10-2	8.5

5. Microstructure analysis

Fig.4a shows the microstructure of BM consisting of elongated grains in α phase with coarse constituents of $CuAl_2$ intermetallic particles is a typical structure of AA2219–T87 alloy (Metals Hand Book1990, Aluminium standards and data1982, Robinson et. al., 1982) Fig.4b shows the SEM images of BM. The presence of $CuAl_2$ particles (white regions) in α-solid solution forms micro galvanic cells with surrounding matrix (Valérie Guillaumin et. al., 1998; Little et. al., 2007) is responsible for the corrosion of BM in sea water.

Fig.5a shows the microstructure of HAZ. The SEM micrograph (Fig.5b) of HAZ clearly shows segregation of $CuAl_2$ intermetallic particles along grain boundaries. Before welding the AA2219 consists of an aluminium rich matrix, α-Al and numerous θ, $CuAl_2$ particles in it. During welding, the temperature in HAZ varies from 490°C to 548°C (eutectic temperature). Due to this welding temperature the fine θ precipitates dissolve and segregate along grain boundaries as higher dense precipitates and remain after cooling. The increasing fraction of $CuAl_2$ particles at the grain boundaries increases the susceptibility to corrosion action with respect to grain matrix (Wislei et. al., 2002; Wislei et. al., 2007). The increased rate of corrosion of HAZ in seawater environment hence is due to the selective dissolution of copper rich intermetallic particles followed by redeposition of copper on the surface matrix.

Fig.6a shows the weld microstructure consisting of a population of copper rich areas in α–solid solution. SEM micrograph (Fig.6b) of WZ exhibits a randomly distributed copper rich area and shrinkage pores. The presence of copper in α-matrix and micro pores is responsible for the higher corrosion rate in WZ when compared to BM.

Fig.4 (a). *Microstructure of base metal*

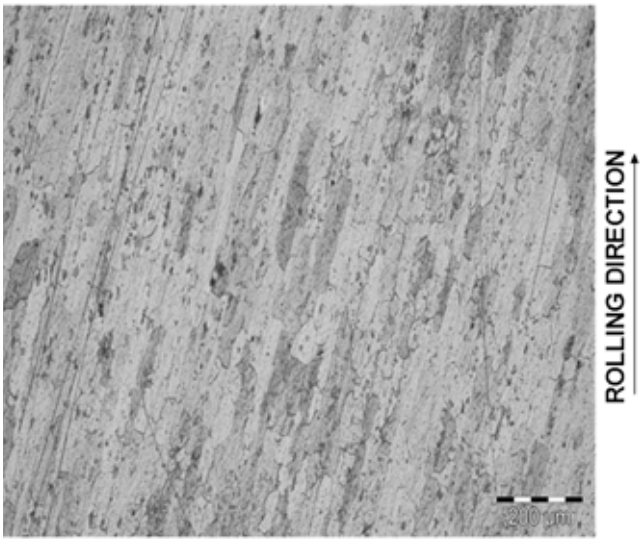

Fig.4 (b). *SEM image of base metal*

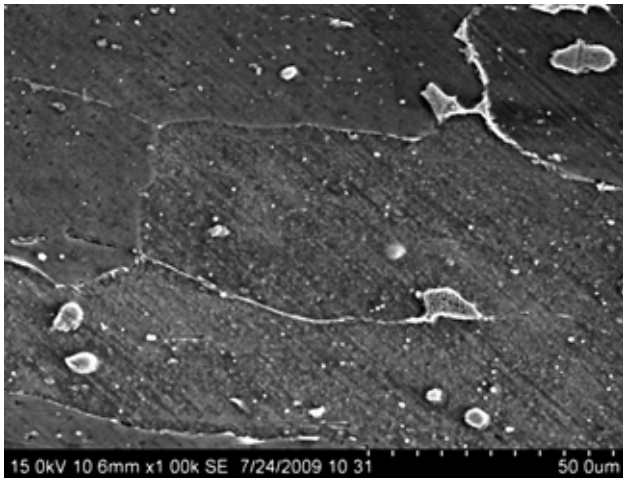

Fig.5 (a). *Microstructure of heat affected zone*

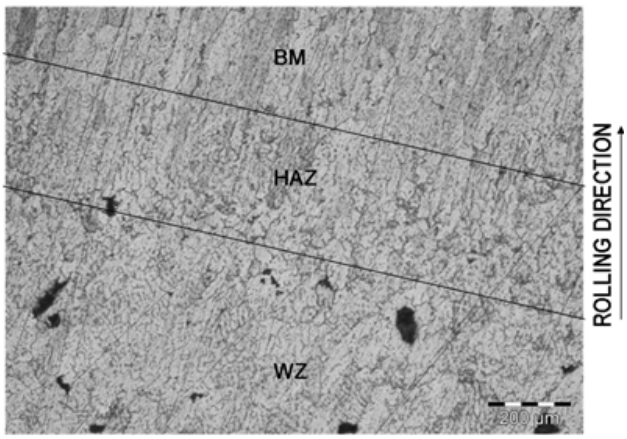

Fig.5 (b). *SEM image of heat affected zone*

Fig.6 (a). *Microstructure of weld zone*

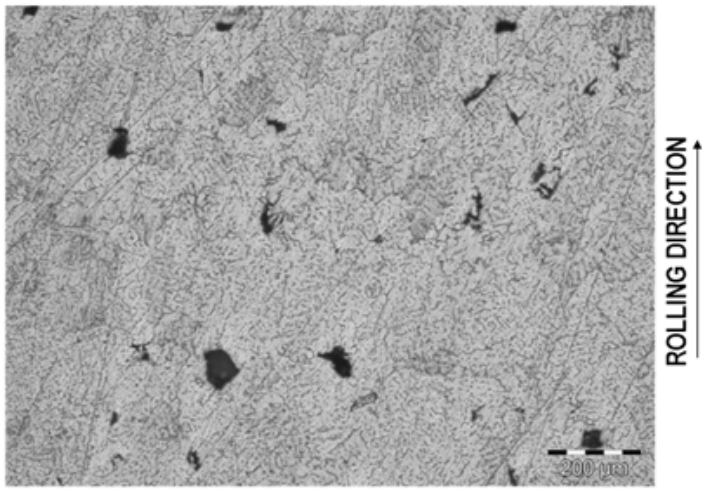

Fig.6 (b). *SEM image of weld zone*

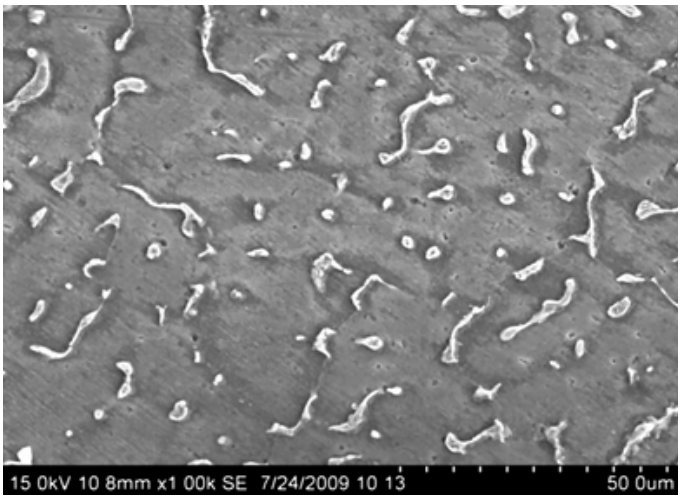

6. Conclusion

In the present work the general corrosion behavior of different zones of AA2219–T87 welded plates in sea water was investigated. Electrochemical results showed that HAZ is more prone to corrosion than WZ and BM.

The results of the microstructural survey performed by SEM confirmed that the increased rate of corrosion of HAZ in seawater is due to the selective dissolution of copper rich intermetallic particles followed by redeposition of copper on the surface matrix. On the other hand, the presence of copper in α-matrix and micro pores is responsible for the higher rate corrosion in WZ when compared to BM.

7. Acknowledgement

The authors are thankful to VSSC, ISRO, Tiruvandram for the grant of this work and for the financial support.

8. References

1. In 'Aluminium standards and data', (1982)159, Washington DC, USA. The Aluminium Association.
2. Standard practice for conventions applicable to electrochemical measurements in corrosion testing, ASTM G3-89 (2004)
3. Balasrinivasan P, Arora K S, Dietzel W, Pandey S, Schaper M K, Characterization of microstructure, mechanical properties and corrosion behavior of an AA2219 friction stir weldment, J Alloys Compd, Vol.492, No.1-2 (2010), pp.631-637.
4. Birbilis N, and Buchheit R G, Electrochemical characteristics of intermetallic phases in aluminum alloys: An experimental survey and discussion, J. Electrochem. Soc., Vol.152, No.4 (2005)B140-B151.
5. Cao G and Kou S, Friction stir welding of 2219 aluminum: Behavior of θ (Al_2Cu) particles, Weld. J., Vol.84, No.1 (2005), pp.1–7.
6. Frankel G S, Xia Z, Localised corrosion and stress corrosion cracking resistance of friction stir welded aluminium alloy 5454, Corrosion, Vol.55, No.2 (1999), pp.139-150.
7. Ghosh B R, Gupta R K, Biju S, Sinha P P, Modified welding technique of a hypo-eutectic Al-Cu alloy for higher mechanical properties, J. Solid Mechs. and Mater. Engg., Vol.1, No.4 (2007), pp.469-479.
8. Hatch J E (Ed.), Aluminum: Properties and physical metallurgy, ASM, Metals Park, OH (1984)242-319.
9. Gnecco.F, Beccaria.A.M., Corrosion behavior of Al-Si/Sic composite in sea water, British Corr. J., Vol.34, No.1 (1999), pp.57-62.
10. Holingsworth E H and Hunsicker H Y, Corrosion of aluminium and aluminium alloys, ASM Hand Book, Vol.13 (2001), pp.583-609.
11. Huang C, and Kou, Liquation cracking in full penetration Al-

Cu Welds, Weld. J. 83, (2) (2004), pp.50-58.

12. Keddam M, Kuntz C, Takenouti H, Schustert D, Zuili D, Exfoliation corrosion of aluminium alloys examined by electrode impedance Electrochim. Acta, Vol.42, No1 (1997), pp.87-97.
13. Koteswara Rao S R, Madhusudhan Reddy G, Srinivasa Rao K, Kamaraj M, Prasad Rao K, Reasons for superior mechanical and corrosion properties of 2219 aluminum alloy electron beam welds, Mater. Charac., Vol.55, No.4-5 (2005), pp.345-354.
14. Kuznicka B, Podrlez M - Radziszewska, Correlation between microstructural evolution in heat affected zone and corrosion behaviour of Al-Cu alloy, Archi. Metall. and Mater., Vol.53, No.3 (2008), pp.933-938.
15. Little D A, B J Connolly and Scully J R, An electrochemical framework to explain the intergranular stress corrosion behavior in two Al–Cu–Mg–Ag alloys as a function of aging Corros. Sci. 49 (2) (2007)347-372.
16. Lumsden J B, Mahoney M W, Pollock G, Rhodes C G, "Intergranular corrosion following friction stir welding of aluminum alloy 7075-T651", Corrosion 5 (1999)1127-1135
17. Lumsden J, Pollock G, Mahoney M, Proc. friction stir welding and processing II, TMS, Warrendale, PA, USA, (2003)99.
18. Lunarska E, Trela E, and Szklarska-smialowska Z, Pitting corrosion of powder metallurgy AlZnMg alloys, Corrosion, Vol.43, No.4 (1987), pp.219-228.
19. Meletis E I and Weiji Huang , The role of the T_1 phase in the pre-exposure and hydrogen embrittlement of Al-Li-Cu alloys, Mater. Sci. and Engg. A, Vol.148, No.2 (1991), pp.197-209.
20. Metals Hand Book, Properties of Aluminium and Aluminium alloys, 10th Ed. Vol.2 (1990), pp.79-80.
21. Paglia C S, Buchheit R G, Microstructure, microchemistry and environmental cracking susceptibility of friction stir welded 2219-T87, Mater. Sci. and Engg. A, Vol.429 (2006), pp.107-114.
22. Paglia C S, Carroll M C, Pitts B C, Reynolds A P, Buchheit R G, Strength, corrosion and environmentally assisted cracking of 7075-T6 friction stir weld, Mater. Sci. Forum, Vol.396 (2002), pp.1677-1684.
23. Paglia C S, Ungaro L M, Pitts B C, Carroll M C, Reynolds A P, Buchheit R G, Proc. friction stir welding and processing II, TMS, Warrendale, PA, USA, (2003)65.
24. Ramgopal T, Gouma P I and Frankel G S, Role of grain boundary precipitates and SDZ on the intergranular corrosion of aluminum alloy AA7150, Corrosion, Vol.58 (2002), pp.687-697.
25. Robinson M J Mathematical modelling of exfoliation corrosion in high strength aluminium Alloys, Corros. Sci., Vol.22, No.8 (1982), pp.775-790.
26. Rossana Grilli, Mark A. Baker, James E. Castle, Barrie Dunn, John F. Watts, Corrosion behavior of a 2219 aluminium alloy treated with a chromate conversion coating exposed to 3.5% NaCl solution, Corros.Sci., Vol.54, No.4 (2011), pp.1214-1223
27. Shibayan Roy, B R Nataraj, Satyam Suwas, S. Kumar, K. Chattopadhyay, Accumulative roll bonding of aluminium alloy 2219/5086 laminates: Microstructural evoluation and tensile properties, Mater. & Desi., (36) (2012)529-539.
28. Valérie Guillaumin and Georges Mankowski, Localized corrosion of 2024 T351 aluminium alloy in chloride media, Corros. Sci. Vol.41, No.3 (1998), pp.421-438.
29. Venkata Narayana G, Sharma V M J, Diwahar V, Sreekumar K, Prasad R C, Fracture behaviour of aluminium alloy 2219–T87 welded plates, Sci. and Tech. of Weld. and Joining, Vol.9, No2 (2004), pp.121-130.
30. Venugopal A, Sreekumar K, Raja VS, Effect of repair welding on electrochemical corrosion and stress corrosion cracking behavior of TIG welded AA2219 aluminium alloy in 3.5% NaCl Solution, Metall Mater Trans A, Vol.41, No.12 (2010), pp.3151-3160.
31. Wang B B, Wang Y Z, Han W, Ke W, Atmospheric corrosion of aluminium alloy 2024-T3 exposed to salt lake environment in Western China, Corros. Sci., (59) (2012)63-70
32. Williams Stewart W, Rajan Ambat, Debbie Price, Manthana Jariyaboon, Alison Davenport J, Andrew Wescott, Laser treatment method for improvement of the corrosion resistance of friction stir welds, Mater. Sci. Forum. Vol.426 (2003), pp.2855-2860.
33. Wislei R. Osório, José E. Spinelli, Alexandre P. Boeira, Célia M. Freire, Amauri Garcia, The influences of macro segregation, intermetallic particles, and dendritic spacing on the electrochemical behavior of hypoeutectic Al-Cu alloys, Micros. Res. and Techniq., Vol.70, No.11 (2002), pp.928–937.
34. Wislei R. Osório , José E. Spinelli, Alexandre P.Boeia, Celia M.Freire, Amauri Garcia, The roles of Al_2Cu and of dendritic refinement on surface corrosion resistance of hypoeutectic Al–Cu alloys immersed in H_2SO_4, J. Alloys and Comp., Vol.443, No.1-2 (2007), pp.87-93.